Supporting Information

Singlet-Triplet Gaps for Evaluating Thermally Activated Delayed Fluorescence: Which One is *the* (b)E_{ST}?

Ali Shuaib[1†], Lubna Salah[2,3†], Antonio Prlj[4], Narendran Rajendran[2], Marc K. Etherington[5], Ahmed Abdel Nazeer[6], Carlito S. Ponseca Jr[7], Andrew P. Monkman[8], Andrew Danos[8,9]*, Saad Makhseed[2]**

[1]Biomedical Engineering Unit, Department of Physiology, Faculty of Medicine, Kuwait University, P.O. Box 24923, Safat-13110, Kuwait
[2]Department of Chemistry, Faculty of Science, Kuwait University, P.O. Box 5969, Safat-13060, Kuwait
[3]Faculty of Chemistry, Silesian University of Technology, Strzody 9, 44-100, Gliwice, Poland
[4]Division of Physical Chemistry, Ruđer Bošković Institute, Bijenička cesta 54, 10000 Zagreb, Croatia
[5]School of Engineering, Physics and Mathematics, Northumbria University, Ellison Place, Newcastle upon Tyne NE1 8ST, UK
[6]Nanotechnology Applications Program, Energy and Building Research Center, Kuwait Institute for Scientific Research, P.O. Box 24885, Safat-13109, Kuwait
[7]Department of Mathematics and Natural Sciences, Gulf University for Science and Technology, Hawally, Kuwait
[8]Department of Physics, Durham University, South Road, Durham DH1 3LE, UK
[9]School of Physical and Chemical Sciences, Queen Mary University of London, London E1 4NS, United Kingdom

*Corresponding authors: ali.shuaib@ku.edu.kw, a.danos@qmul.ac.uk, saad.makhseed@ku.edu.kw
†These authors contributed equally to this work

Contents

1. General Methods

All reagents were used without further purification unless otherwise specified. 5,6-Dichloro-2,3-dicyanopyrazine {CAS No. 56413-95-7} and 3,6-di-tert-butylcarbazole{CAS No. 37500-95-1} were purchased from Sigma-Aldrich. TLC was performed using Polygram sil G/UV 254 TLC plates and visualization was carried out by ultraviolet light at 254 nm and 350 nm. Anhydrous solvents were either supplied from Sigma-Aldrich or dried as described by Perrin[1]. ^{1}H and ^{13}C NMR Spectra were recorded using Bruker DPX 600 at 600 MHz. IR spectra were obtained from Jasco FT/IR 6300. UV-Vis studies were performed on a Cary 60 UV-Vis spectrophotometer (Agilent). Melting points were determined via differential scanning calorimetry (DSC) analyses on a Shimadzu DSC-50. Thermal analysis was determined using a Shimadzu DTG-60 thermogravimetric analyser and a TMA-60H thermomechanical analyser.

Solutions were prepared at 10 μM concentration for absorption and photoluminescence measurements. Zeonex and DPEPO/PPT films were drop-cast from a mixture of the fluorophore and host in toluene at the stated weight percentage and deposited onto pre-heated quartz substrates on a hot plate (70° C). The films were placed in a cryostat (Janis VNF-100) and the measurements performed in vacuum at room-temperature and under an inert nitrogen gas atmosphere at low-temperature.

Steady-state fluorescence spectra measurements were performed using a HORIBA Fluorolog 3 or Edinburgh Instrument FLS980 spectrometer. Fluorescence (PF and DF) and phosphorescence (PH) spectra and decays were recorded by nanosecond gated luminescence and lifetime measurements (from 400 ps to 1 s) using a pulsed Nd:YAG laser (355 nm, EKSPLA, ~100 μJ/cm^2). Emission was focused onto a spectrograph and detected on a sensitive gated iCCD camera (Stanford Computer Optics) of subnanosecond resolution. PF/DF time-resolved measurements were performed by exponentially increasing gate and delay times.

The electrochemical properties of **4CzPyz** and **4tCzPyz** were studied by cyclic voltammetry (CV) under inert atmosphere using glassy carbon electrode (GCE) as working electrode, platinum wire as counter electrode and saturated calomel electrode (SCE) as reference electrode. A 0.1 M Tetrabutyl ammonium hexafluorophosphate ($TBAPF_6$) solution used as supporting electrolyte with concentration of 1×10^{-4} mol L^{-1} of the investigated compound, at a scan rate of 100 mV s^{-1}. Prior to the CV scans, the GCE was polished with alumina (< 10 μm) on a Buehler felt pad, followed by washing with deionized (DI) water and rinsing with methanol and dichloromethane (DCM).

Electronic structure, geometry optimizations, and normal mode frequency calculations were performed using the Turbomole 7.8 package.[2] The structures of **4CzPyz** and **4tCzPyz** in their lowest triplet states were optimized with density functional theory (DFT) employing the PBE0 functional,[3] Grimme's D3 dispersion correction with Becke–Johnson damping,[4] and the def2-SVP basis set[5] (i.e., PBE0-D3BJ/def2-SVP level). For both compounds, only the conformer corresponding to crystal structure was considered (conformer B in our previous work[6], see Fig. S57 therein).

Nuclear ensembles were sampled from a harmonic Wigner distribution[7] at 80K, using the normal mode frequencies calculated with DFT. For **4tCzPyz**, the lowest frequency mode of only 1.2 cm^{-1} was excluded from the sampling, as it produced a subset of unphysical geometries (note that this is a common practice when dealing with anharmonic and low-frequency modes[9]). For each compound, we sampled 500 structures and used them for subsequent excited-state calculations.

Excitation energies of the S_1 and T_1 states were calculated for 500 structures of each compound, using time-dependent DFT within the Tamm–Dancoff approximation at the PBE0-D3BJ/def2-SVP level. These energies were then subtracted to access ΔE_{ST}values on a per-molecule basis. This level of theory has previously shown good agreement with correlated wavefunction-based reference method for the 4CzPyz compound.[6]

2. Synthetic Methods

Synthesis: Synthesis of 2,3,5,6-Tetrakis(9-carbazolyl)pyrazine (**4CzPyz**)

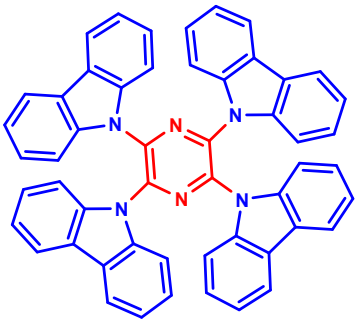

4CzPyz

4CzPyz was previously reported in the literature[6]. The material was obtained as a light green solid with a melting point of 453–454 °C. ^{1}H NMR (400 MHz, DMSO-d6) δ 7.99 (m, 8H, H6), 7.81 (m, 8H, H3), 7.16 (m, 16H, H4+5). ^{13}C NMR (151 MHz, DMSO-d6) δ 139.6 (C1), 138.6 (C2), 125.7 (C4), 123.5 (C7), 121.2 (C5), 120.1 (C6), 111.4 (C3).

Synthesis: Synthesis of 2,3,5,6-tetrakis(3,6-di-tert-butyl-9H-carbazol-9-yl) pyrazine (**4tCzPyz**)

A 100 mL round bottom flask equipped with a nitrogen atmosphere was introduced with 5,6-dichloropyrazine-2,3-dicarbonitrile (1 g, 5 mmol, 1.0 equiv.) in anhydrous DMF (30 mL) followed by the slow addition of NaH (60% suspension in mineral oil) (1.6 g, 40 mmol, 8 equiv.) to initiate anion generation. The calculated amount of 3,6-di-tert-butyl-9H-carbazole (11.23g, 40 mmol, 8 equiv.) was added to the reaction mixture and stir the reaction vigorously at room temperature for 48 h. After completion of the reaction, the reaction mixture was poured into a 1M HCl solution resulting in a yellow precipitate crashing out. The bright yellow solid was filtered off, followed by washing the filtrate several times with water (3 × 100 mL). This yellow solid was purified by refluxed with methanol (3 × 100 mL) and carefully dried using vacuum oven at 80°C. Yield: 40%; m.p.: > 300 °C. IR/cm^{-1} (KBr): 2961 (aliphatic C-H stretching), 1471, 1298, 1183 (pyrazine ring stretching frequencies); ^{1}H NMR (600 MHz, $CDCl_3$) δ (ppm): 7.66 (d, J=1.8 Hz, 1H), 7.31 (dd, J = 1.2, 9 Hz, 1H), 6.89 (dd, J = 1.2 Hz, 7.2 Hz, 1H); ^{13}C NMR (150 MHz, $CDCl_3$) δ (ppm): 144.32, 136.91, 135.56, 124.81, 123.57, 115.50, 110.74, 34.76, 32.03.

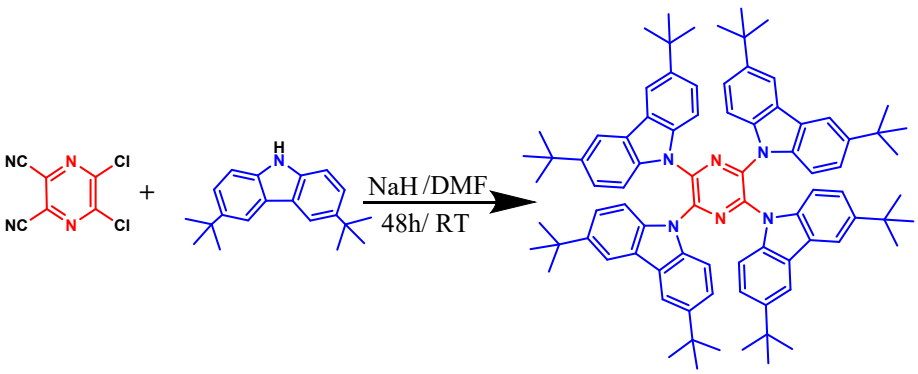

scheme S1: Synthetic route used to prepare **4tCzPyz**.

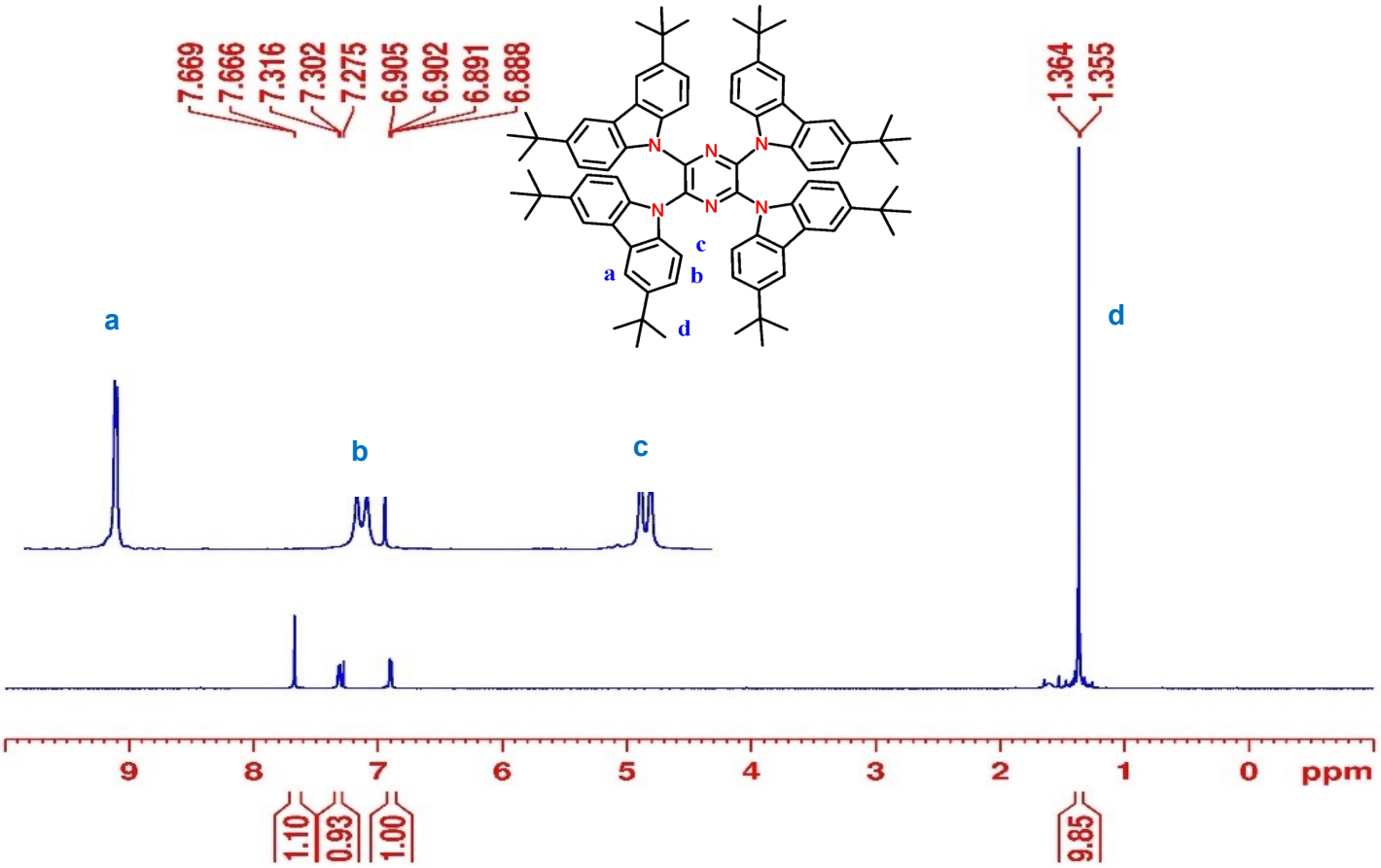

3. ^{1}H and ^{13}C NMR Spectroscopic Characterisation of Synthesized Compound

Figure S1: ^{1}H-NMR **4tCzPyz** in $CDCL_3$.

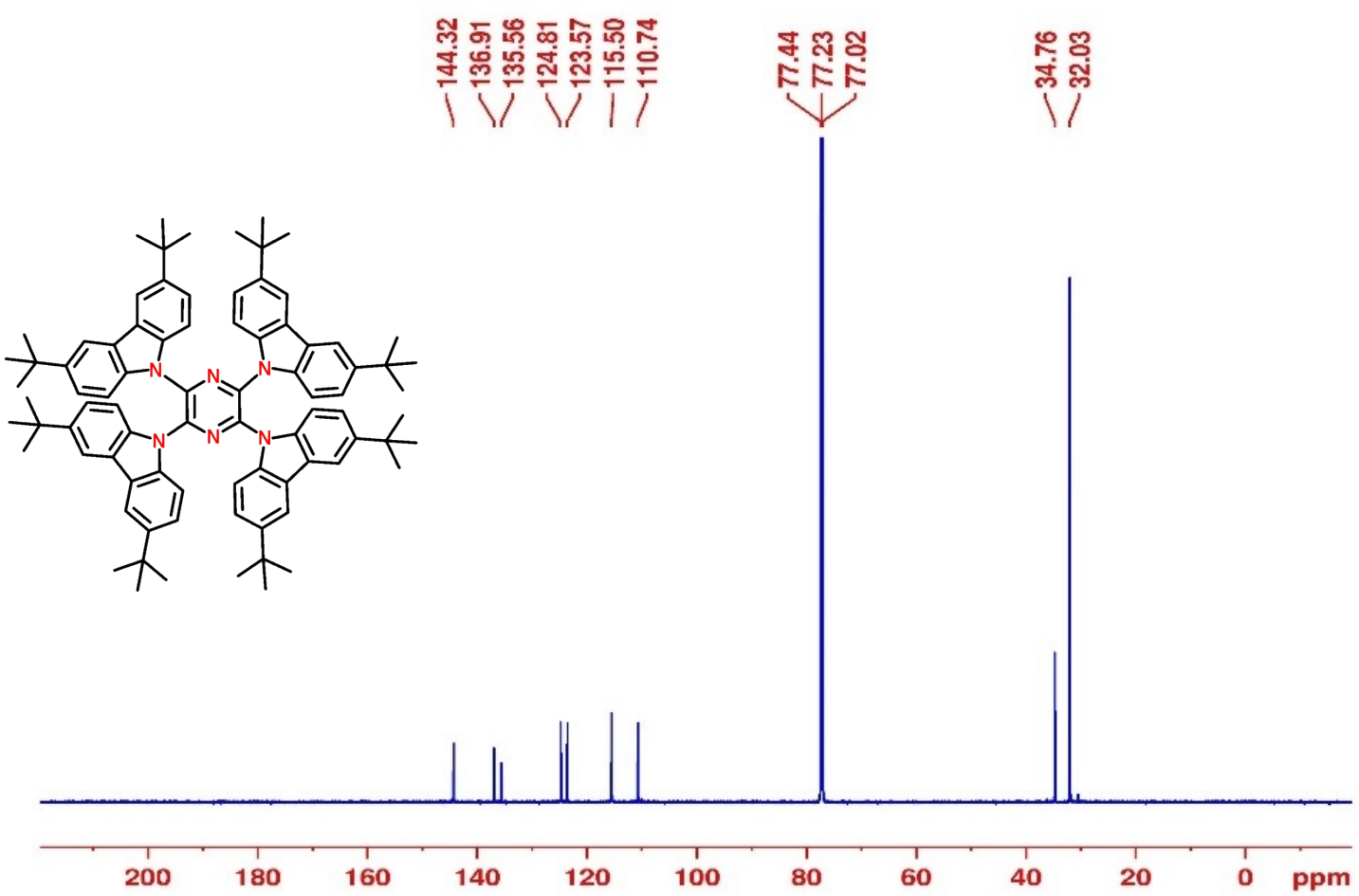

Figure S2: ^{13}C-NMR of **4tCzPyz** in $CDCL_3$.

4. Thermogravimetric Analysis (TGA)

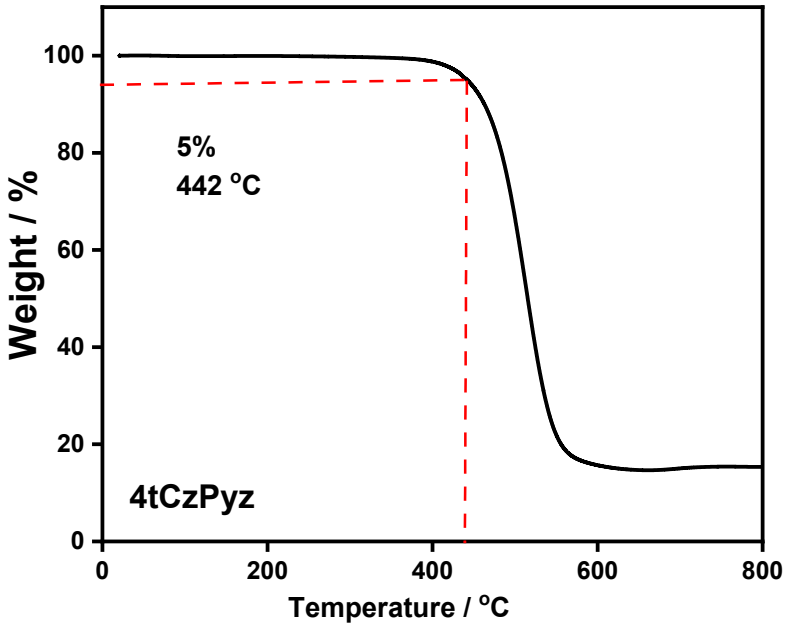

Figure S3: Thermogravimetric analysis Profiles of Compound **4tCzPyz**.

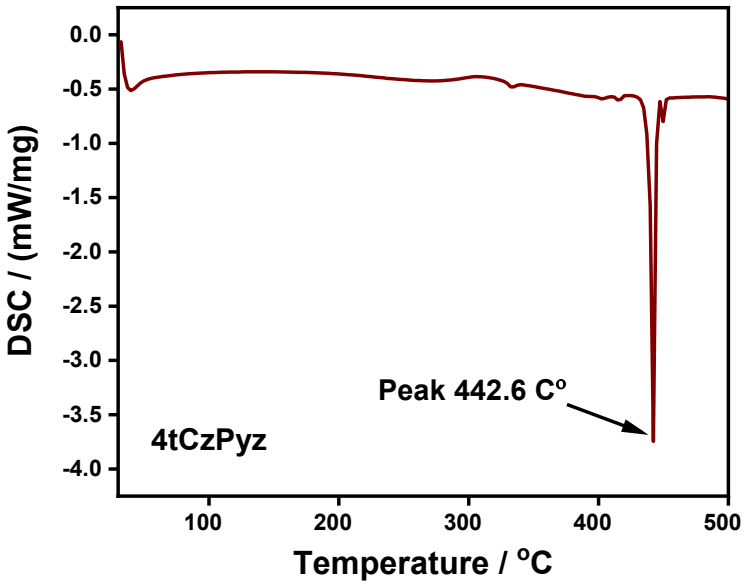

Figure S4: Differential scanning calorimetry profiles of compounds **4tCzPyz.**

5. Fourier transform infrared spectroscopy (FTIR) Spectral Profiles

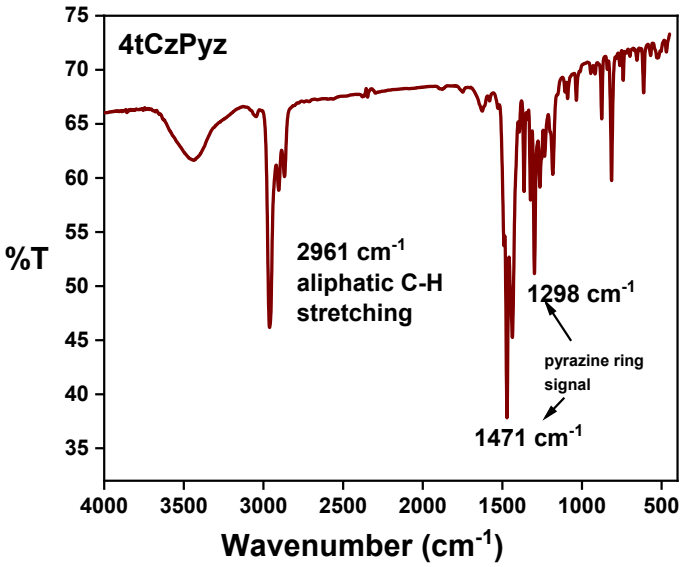

Figure S5: FTIR spectrum of **4tCzPyz** by KBr pellet method.

6. Cyclic Voltammetry (CV)

The electrochemical behavior of **4CzPyz** and **4tCzPyz** was assessed using cyclic voltammetry in DCM solution versus SCE using ferrocene as internal standard and TBAPF6 as supporting electrolyte, as shown in **Figure S6**. Values of the half-wave potential of the oxidation and reduction processes, HOMO, LUMO, and the energy gap (E_g) are listed in **Table S1**.

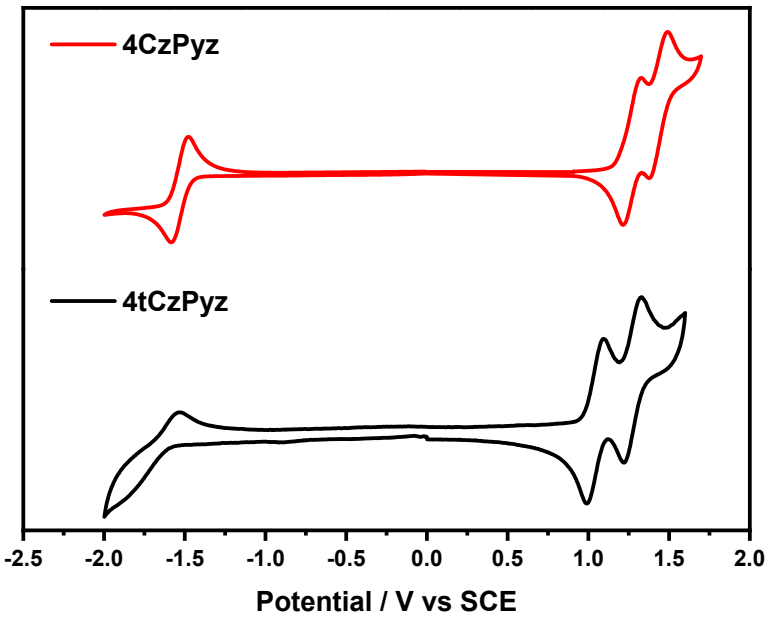

Figure S6: Cyclic voltammograms **4CzPyz** and **4tCzPyz** in DCM/0.1 M TBAPF6 at scan rate 100 mVs^{-1}.

Table S1: Electrochemical data of **4CzPyz** and **4tCzPyz** in DCM.

Compounds	E_{oxd1}/V SCE	E_{oxd2}/V SCE	E_{red1}/V SCE	HOMO (eV)	LUMO (eV)	E_g
4CzPyz	1.19	1.40	-1.47	-5.59	-2.93	2.66
4tCzPyz	1.03	1.24	-1.61	-5.43	-2.79	2.64

The HOMO energy level for these compounds was determined from their onset of the first oxidation potentials which localized on the carbazole moiety (electron-donating unit), while the LUMO energy level localized at the pyrazine ring (electron-deficient unit), demonstrating that these compounds could exhibit a bipolar character. Within the electrochemical window of DCM/$TBAPF_6$ electrolyte system, both **4CzPyz** and **4tCzPyz** showed two reversible oxidation peaks and one quasi-reversible reduction peak. The chemical reversibility for **4CzPyz** and **4tCzPyz** was pronounced according to the ratios of peak currents, which are close to unity at

different scan rates, as shown in **Figure S7**. All reduction waves could be assigned to the pyrazine ring due to its electron-deficient feature.

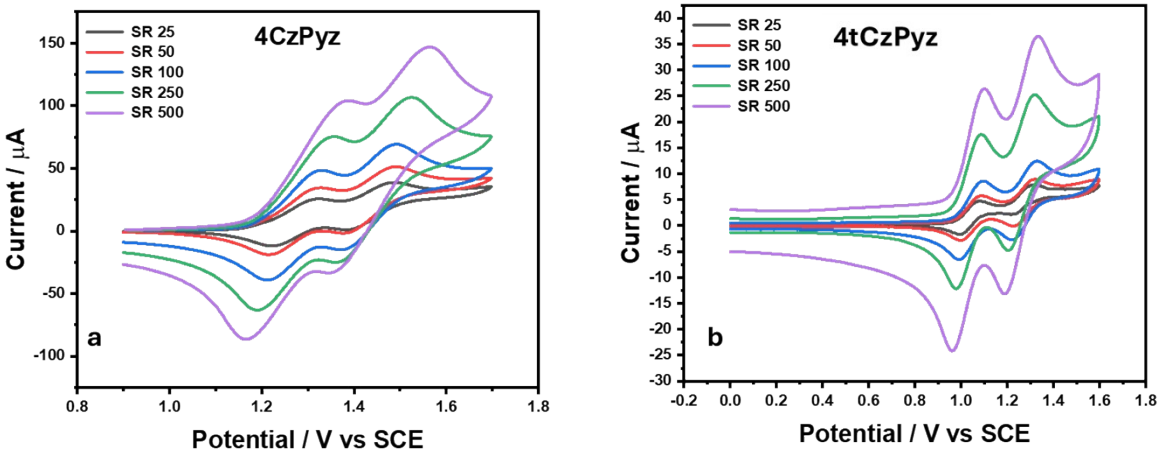

Figure S7: Cyclic voltammograms of (a) **4CzPyz** and (b) **4tCzPyz** at different scan rates.

Figure S8 showed that **4CzPyz** and **4tCzPyz** maintained their electrochemical stability with cycling, making these pyrazine derivatives suitable for use in electrochromic devices (ECDs) applications.

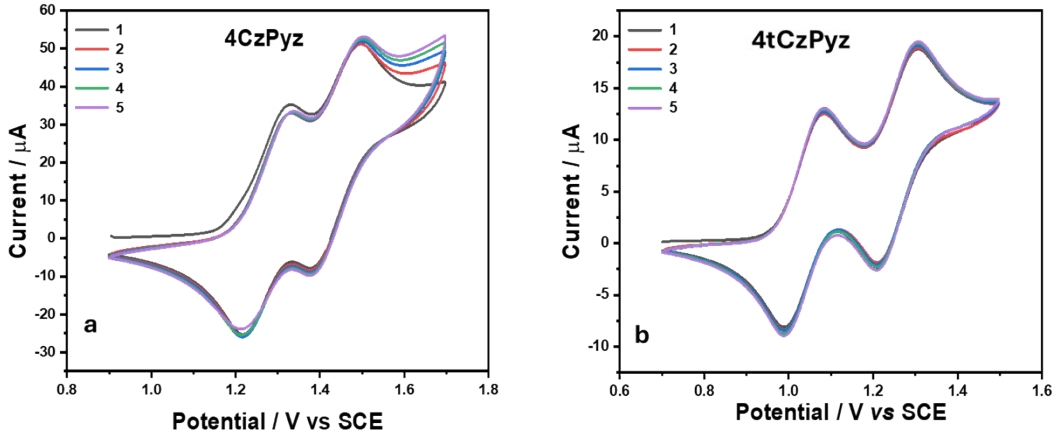

Figure S8: Cyclic voltammograms for (a) **4CzPyz** and (b) **4tCzPyz** for different cycles at scan rate 50 mVs^{-1}

From **Table S1**, it can be well illustrated that **4CzPyz** has a low onset oxidation potential and hence a low HOMO energy level due to the presence of four electron-donating carbazole units, which can decrease the electron deficiency of the pyrazine ring and subsequently decrease the HOMO energy level. In the case of the **4tCzPyz**, a lower onset oxidation potential was recorded (lower HOMO), which is associated with the introduced tert-butyl groups to the carbazole units that enhance their electron-donating abilities. Also, **4tCzPyz** showed a lower electron-deficient character distinguished with a higher reduction potential at -1.61 mV.

References:

(1) Perrin, D. D.; Armarego, W. L. F. *Purification of Laboratory Chemicals*, 3rd ed.; Pergamon Press: Oxford, 1988.

(2) Balasubramani, S. G.; Chen, G. P.; Coriani, S.; Diedenhofen, M.; Frank, M. S.; Franzke, Y. J.; Furche, F.; Grotjahn, R.; Harding, M. E.; Hättig, C.; Hellweg, A.; Helmich-Paris, B.; Holzer, C.; Huniar, U.; Kaupp, M.; Khah, A. M.; Khani, S. K.; Müller, T.; Mack, F.; Nguyen, B. D.; Parker, S. M.; Perlt, E.; Rappoport, D.; Reiter, K.; Roy, S.; Rückert, M.; Schmitz, G.; Sierka, M.; Tapavicza, E.; Tew, D. P.; van Wüllen, C.; Voora, V. K.; Weigend, F.; Wodyński, A.; Yu, J. M. TURBOMOLE: Modular program suite for ab initio quantum-chemical and condensed-matter simulations. *J. Chem. Phys.,* **2020**, 152, 184107. https://doi.org/10.1063/5.0004635

(3) Adamo, C.; Barone, V.; Toward reliable density functional methods without adjustable parameters: The PBE0 model. *J. Chem. Phys.,* **1999**, 110, 6158–6170 https://doi.org/10.1063/1.478522

(4) Grimme, S.; Ehrlich, S.; Goerigk, L.; Effect of the damping function in dispersion corrected density functional theory. *J. Comput. Chem.*, **2011**, 32: 1456-1465. https://doi.org/10.1002/jcc.21759

(5) Weigend, F.; Ahlrichs, R.; Balanced basis sets of split valence, triple zeta valence and quadruple zeta valence quality for H to Rn: Design and assessment of accuracy, *Phys. Chem. Chem. Phys.*, **2005**,7, 3297-3305 https://doi.org/10.1039/B508541A

(6) Salah, L.; Etherington, M. K.; Shuaib, A.; Danos, A.; Nazeer, A. A.; Ghazal, B.; Prlj, A.; Turley, A. T.; Mallick, A.; McGonigal, P. R.; Curchod, B. F. E.; Monkman, A. P.; Makhseed, S. Suppressing Dimer Formation by Increasing Conformational Freedom in Multi-Carbazole Thermally Activated Delayed Fluorescence Emitters. *J. Mater. Chem. C,* **2021**, *9* (1), 189–198. https://doi.org/10.1039/D0TC04222F.

(7) Hillery, M. A.; O'Connell, R. F.; Scully, M. O.; Wigner, E. P.; Distribution Functions in Physics: Fundamentals, *Phys. Rep.,* **1*984***, 106, 121 https://doi.org/10.1016/0370-1573(84)90160-1

(8) David Tannor, *Introduction to Quantum Mechanics : A Time-Dependent Perspective*, 2008

(9) Prlj, A.; Hollas, D.; Curchod, B. F. E. Deciphering the Influence of Ground-State Distributions on the Calculation of Photolysis Observables. *J. Phys. Chem. A,* **2023**, *127*, 7400–7409, DOI: 10.1021/acs.jpca.3c02333